HiSST: 3rd International Conference on
High-Speed Vehicle Science Technology
14 -19 April 2024, Busan, Korea

AERO-THERMAL STUDY AND EXPERIMENTAL CHARACTERIZATION OF A NOVEL OPTICAL PROBE FOR HIGH TEMPERATURE SUPERSONIC FLOWS

Ignacio Lasala[1], Aubrey McKelvy[1], Guillermo Paniagua[1], Etienne Choquet[2], Thierry André[2], François Falempin[2]

Abstract

This manuscript details the thermal design, analysis, and experimental characterization of a cooled aerodynamic probe to house sensitive instrumentation for diagnostics in high-enthalpy environments up to $M_1 = 6$ and $T_{01} = 1700\ K$. The probe is cooled using an open cycle gaseous cooling jacket terminating in a pattern of backward oriented ejection holes. The cooling jacket has been sized using a 1D heat transfer model and requires a head pressure of 3 bar to satisfy the thermal limits of the stainless-steel walls (800 K) and enclosed instrumentation (315 K). The effusion cooling effectiveness of the probe is further characterized through a parametric study using 3D steady RANS simulations from subsonic to high supersonic conditions. Experimental tests have been conducted in an underexpanded open jet at $M_1 = 1.07$ and T_{01} = 370 K using "in-situ" calibrated Infrared thermography to resolve the conjugate cooling effectiveness of the probe across the effusion faces. Cooling patterns observed in the effusion faces in simulations at $M_1 = 6$ are observed in the transonic test under similar pressure ratios, and the conjugate cooling effectiveness agrees with computational predictions.

Keywords: *Optical-probe, supersonic-flow, cooling-effectiveness, infrared-thermography, RANS*

Nomenclature

Latin
BR – Blowing ratio [-]
D – Diameter [m]
h – heat transfer coefficient [W/(m^{2}K)]
k – Thermal conductivity [W/(mK)]
M – Mach number [-]
Nu – Nusselt number [-]
P – Pressure [bar]
Pr – Prandtl number [-]
q̇ – Heat flux [W/m^2]
Re – Reynolds number [-]
T – Temperature [K]
U – Velocity [m/s]
z – Pitch between holes [m]
Greek
η – Cooling effectiveness [-]
ρ – Density [kg/m^3]
Subscripts
1 – Free stream properties
2 – Properties downstream normal shock
ad – Adiabatic
cj – Conjugate
w – Relative to the wall

[1] *Maurice J. Zucrow Laboratories, Purdue University, West Lafayette, IN, USA*
[2] *MBDA, Le Plessis Robinson, France*

1. Introduction

Research in high-enthalpy supersonics is generally constrained by the instrumentation access of the facilities, in which the severe conditions faced inhibit the use of multiple access ports and optical windows, restricting the measurable area [1][2]. Modifying the facilities to tailor instrumentation access is costly and even unfeasible depending on the structural requirements, necessitating from a new approach to expand the measurable region. Inman et al. introduced redirecting optics inside high-enthalpy supersonic test sections to tailor optical access [3], and despite their success, they reported problems with optical alignment as the optics were directly exposed to the free stream. In this study, a modular probe is presented with an internal 980 cm^3 cavity able to encapsulate sensitive instrumentation such as redirecting optics for laser-based measurement techniques and keep them isolated from the free stream. Additionally, the probe has a "ship's bow" shape to deviate the perturbed streamlines downwards and minimize flow disturbance above and in front of it, where the measurements are taken. The probe needs to withstand the thermal environment of the facility while keeping the internal instrumentation within its operating range. It is designed to survive in M_1 = 6, T_{01} = 1700 K and P_{01} = 45 bar flow and requires a maximum temperature in the cavity below 315 K to allow the use of motorized components for displacing instrumentation and optical hardware, enhancing the versatility in selecting the location of the measurement. These requirements necessitate an ad-hoc cooling system with minimized implications in the aerodynamics of the probe.

Brouckaert et al. [4] designed an internal, closed-cycle cooling jacket for a pressure probe in T_{01} = 1400 K and P_{01} = 40 bar flows. Despite the ability to cool the internal cavity, they reported limitations for cooling the external walls due to the low thermal conductivity of typical structural materials. Open-cycle cooling schemes provide further cooling by ejecting the coolant to the exterior at the end of its path. However, the downstream and spanwise effect of the ejected coolant decays rapidly with distance from the ejection hole [6]. By increasing the number of holes and reducing their spacing, an effusion system is achieved with more homogeneous cooling effectiveness, which is used in gas turbine combustors where the flow can exceed 2000 K [7]. This configuration can reach near maximum cooling effectiveness with low blowing ratios, reducing jet penetration and flow distortion, which are key features to account when designing a probe. Chuvakhov additionally shown that backward ejection minimizes pressure losses and flow distortion in high-supersonic environments [8]. It also requires lower cooling pressures than frontward ejection and avoids the nonuniform ejection behavior seen by Lozano and Paniagua due to Coanda effect [9], motivating the use of this scheme.

This study presents the design and assessment of a mixed convective-effusive cooling system for a novel optical probe able to operate within high-temperature, high-Mach flows. A combined strategy based on 1D modelling, 3D steady RANS simulations and experimental testing is followed to characterize the cooling behavior of the probe across all its operating envelope and study it as a function of blowing and pressure ratios. The conducted research shows the agreement between both three methods and validates the efficacy of the cooling scheme.

2. Probe and cooling architecture

2.1. Design guidelines

The probe is intended to operate across a range of conditions spanning from subsonic to supersonic high temperature flows up to $M_1 = 6$ and $T_{01} = 1700$ K. The aerodynamic design is detailed by McKelvy [10] and aims to minimize flow distortion in front of and above the probe. The "ship's bow" shape deviates the flow downwards by Coanda effect using a leading-edge sweepback angle of 30º. The flat top surface reduces the effective blockage and the bow shock angle above the probe, as verified with 3D RANS CFD [10]. For cooling, air or gaseous nitrogen are injected through the aft body of the probe and routed around the exterior of the cavity, isolating the cavity from the external walls to keep its temperature below 315 K. An open cycle gaseous scheme is selected to avoid the complexity of watertight liquid schemes and enables to eject the coolant at the end of the path. This is done through 698 1mm diameter effusion holes that generate a coolant film that builds above the external walls providing further isolation and cooling effectiveness. The effect of the ejected coolant in flow distortion is minimized by using backward oriented holes with coolant pressures near the lowest one that satisfies the temperature requirements of the cavity and the walls. The thermal limit of the walls depends on the material, which is selected from a 1D heat transfer model that also sets the channel dimensions and aspect ratio. Fig. 1 shows a section view of the probe and the cooling scheme.

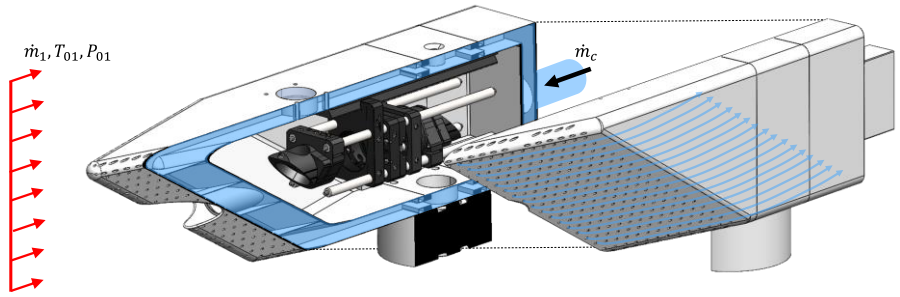

Fig 1. Section view of the developed probe and cooling architecture

2.2. 1D Heat transfer model

The cooling jacket is sized iterating through of a 1D steady-state heat transfer scheme. The coolant path is first discretized in parcels for which heat flux equilibrium across the walls is imposed. For the external wall, the convective heat transfer with the hot flow is modelled using a Reynolds analogy-based correlation for local Nusselt number across flat plates Nu_x (Eq 1) [11], and heat transfer with the coolant using Dittus-Boelter correlation for average Nusselt number in internal flows Nu_D (Eq 1) [12]. The Nusselt number allows to compute the heat transfer coefficient h (Eq 1). Conduction across the external wall is accounted but it yields a negligible temperature difference between both sides due to its small thickness (~0.8-1 mm). For the internal wall, at the side of the cooling channel in contact with the cavity, an adiabatic condition is used for closing the problem making the cavity temperature equal to the wall temperature, which is a conservative condition as it assumes that the cavity is not further cooled by natural convection. The steady-state problem is solved by iterating the value of the external wall temperature until heat flux equilibrium is reached at both sides. The heat load found in a parcel is used to update the coolant temperature at the next one until the cooling path is covered. Fig. 2a shows a schematic of the heat transfer problem in a generic parcel.

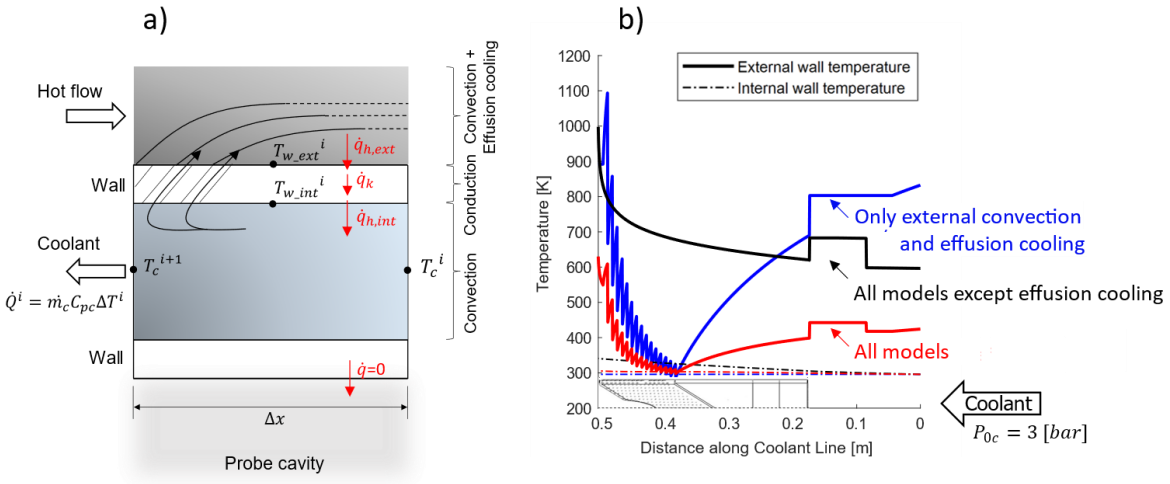

Fig 2. Schematic of the heat transfer problem solved at each coolant parcel (a) and wall temperatures achieved accounting for different heat transfer mechanisms (b).

$$\mathrm{Nu_x} = 0.0296 \cdot \mathrm{Re_x}^{4/5} \cdot \mathrm{Pr}^{1/3} \qquad \mathrm{Nu_D} = 0.023 \cdot \mathrm{Re_D}^{4/5} \cdot \mathrm{Pr}^{0.4} \qquad \mathrm{h} = \frac{\mathrm{Nu\ k}}{\mathrm{L}} \tag{1}$$

$$\eta_{\mathrm{ad,i}} = \frac{C_1}{\xi^{C_2}} \rightarrow C_1 = 1.193 \rightarrow C_2 = 0.5809 \rightarrow \xi = \frac{4}{\pi}\frac{\frac{X}{D_h}\frac{z}{D_h}}{BR} \qquad \eta_{\mathrm{ad}} = 1 - \prod_{i=1}^{n}(1-\eta_{\mathrm{ad,i}}) \qquad \eta_{\mathrm{ad}} = \frac{T_{\mathrm{ad}} - T_r}{T_{0c} - T_r} \tag{2}$$

The effect of effusion cooling in reducing the external wall temperature is modelled using a correlation proposed by Colban et al. [13] for the spanwise averaged adiabatic cooling effectiveness

$\eta_{ad,i}$ for a column "i" of holes (Eq 2). Seller's model is used to account for the combined effect of several columns of holes axially distributed (Eq 2) [14]. From η_{ad} one can compute the updated adiabatic wall temperature T_{ad} knowing the recovery temperature T_r (Eq 2) and use it to calculate the heat flux. Fig. 2b illustrates the results for the probe in a $M_1 = 6$, $T_{01} = 1700$ K, $P_{01} = 45$ bar stream for a final cooling channel height of 1 cm, channel aspect ratio of 2, initial coolant temperature of 300 K and a total coolant pressure of 3 bar considering the different heat transfer mechanisms indicated in Fig. 2a. The first 0.18 m represent piping for delivering coolant to the plenum (right of the plot) and the position x = 0.51 m corresponds to the tip of the probe.

Fig. 2b shows that effusion cooling drastically changes the cooling behavior. If not accounted, a coolant pressure of 3 bars reduces the temperature in most parts of the walls to ~700K, but stagnation point heating in the tip makes it reach 1000 K. Further analysis has shown that a coolant pressure of at least 10 bar would be needed to reduce the tip temperature below 700 K without considering effusion cooling. When only effusion cooling is modelled to act against external convection, a dramatic reduction in wall temperature is produced at the end of the effusion faces (x = 0.4 m), where the wall temperature is almost equal to the coolant temperature ($\eta_{ad} \sim 1$). However, effusion cooling alone does not help cooling enough the tip. When all models are considered, internal convection helps reduce the temperature in those regions in which effusion cooling loses effectiveness, yielding a temperature distribution that is always below 700 K for a moderate cooling pressure of 3 bar. The internal wall temperature is always lower than 315 K, satisfying the limit of the cavity. The results were obtained for stainless steel 316L, which was selected for the probe body as its thermal limit is 800 K and facilitates the manufacture of the complex-shaped probe using 3D printing. It also brings the potential of using even lower cooling pressures to keep the probe below 800 K, but this needs further investigation. However, effusion cooling is a complex phenomenon, Goldstein [15] collects numerous correlations that give different cooling behaviors with small changes in hole geometry and orientation. Thus, numerical computations are performed in this study to further characterize the effusion cooling effectiveness of the probe and verify the drastic benefit predicted by the 1D model.

3. Computational study of the effusion cooling scheme

3.1. Numerical approach

The effect of effusion cooling is studied numerically using Metacomp CFD++ software [16]. Simulations ranging from subsonic to $M_1 = 6$ are conducted. Despite the high Mach numbers, the studied range is within the limit at which the ideal–calorically perfect gas model is valid [17][18] and conventional Navier-Stokes equations can still be adopted due to thermomechanical equilibrium [19]. The k-ω SST model has been used for turbulence closure due to its accuracy in near-wall calculations. The domain has been discretized using Hexpress from Numeca and a symmetry boundary condition is used in the middle plane to reduce the computational time. The highest Y+ was found in the Mach 6 simulations and was below 1. Grid independence was achieved for a mesh of 15.6 million cells as less than 0.1% variation in drag and 1% variation in heat flux were found when compared to a further refined mesh of 21 million cells. The domain and boundary conditions are shown in Fig. 3a and the grid in Fig. 3b.

The free stream flow enters by the left boundary in Fig. 3a in subsonic, transonic, or supersonic conditions, where total pressure and temperature are imposed. A free jet configuration is modelled where all the other boundaries are outlets to avoid unstarting [20]. In the subsonic simulations an ambient back pressure is selected whereas in the supersonic cases the outlet conditions are propagated from upstream information. The domain does not include the internal geometry of the probe, but all the cooling holes are modelled as pressure inlets to enable flow ejection and study the effect of effusion cooling for different coolant total pressures. The coolant temperature was fixed at 315 K as it is the limiting temperature of the internal cavity. Adiabatic boundaries are used to analyze the adiabatic effusion cooling effectiveness, defined in Eq 3. The most relevant inputs are displayed in Table 1.

$$\eta_{ad} = \frac{\left(T_{w\_ad}\right)_{cooled} - \left(T_{w\_ad}\right)_{uncooled}}{T_{0c} - \left(T_{w\_ad}\right)_{uncooled}} \tag{3}$$

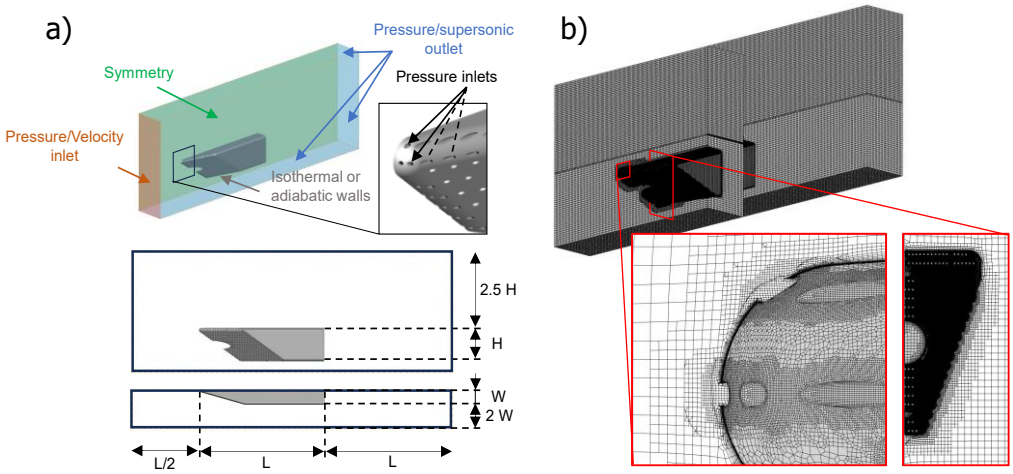

Fig 3. Numerical domain with relative dimensions and boundary conditions (a) and mesh with close-up view of the effusion holes and the cross-section (b).

Table 1. Main flow, coolant and wall conditions for the numerical simulations

M_1 $(-)$	P_{01} (bar)	T_{01} (K)	P_{0c} (bar)	T_{wall} (K)
0.3	1.07	560	[1-2]	Adiabatic
1.5	3.67	810	[1.4-6]	Adiabatic
3	36.7	1570	[3-8.1]	Adiabatic
4	4.37	870	0.73	Adiabatic
4.5	8.34	1040	0.86	Adiabatic
5	15.24	1240	[1-1.38]	Adiabatic
5.5	26.91	1460	1.15	Adiabatic
6	44.52	1700	[0.13-3.99]	Adiabatic

3.2. Adiabatic cooling effectiveness

Fig. 4 depicts the η_{ad} contours for the limiting design point ($M_1 = 6, T_{01} = 1700\ K, P_{01} = 45\ bar$) at four pressure ratios $P_{0c}/P_{02} = [0.55, 0.75, 2, 3]$, where P_{02} is the total pressure downstream of the normal shock formed at the tip, yielding ejection pressures of $P_{0c} = [0.57, 0.78, 2.6, 3.9]$ bar.

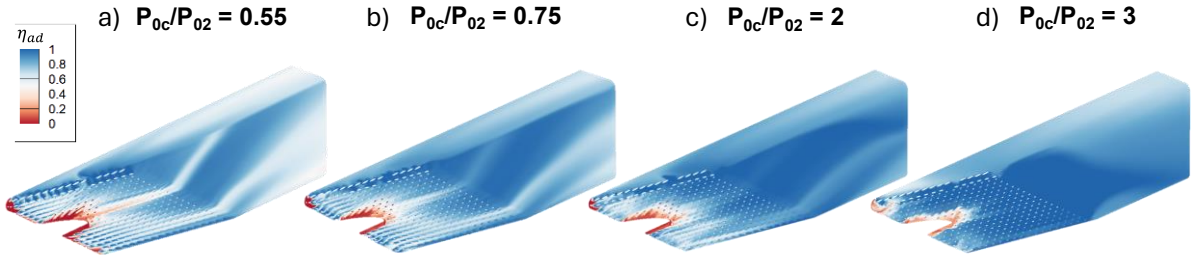

Fig 4. Adiabatic cooling effectiveness at a total pressure ratio P_{0c}/P_{02} of 0.55 (a), 0.75 (b), 2 (c) and 3 (d) for $M_1 = 6$.

Fig. 4a shows that for total pressure ratios lower than unity the cooling holes facing forward are not able to overcome the stagnation pressure of the flow downstream of the bow shock and are not ejecting. However, as most of the holes in the lateral faces are facing sideways, they only need to overcome the static pressure to start ejecting, generating regions of near maximum effectiveness even at low cooling pressures. The interaction between the hot flow and the front window for optical access prevents the cooling holes immediately downstream from overcoming the flow pressure, generating a streak of non-ejecting holes with a corresponding hot region that propagates further downstream. When the pressure ratio is increased to 0.75 (Fig. 4b) the holes below the tip start ejecting as they are not directly facing the stagnation pressure and can eject even for $P_{0c}/P_{02} < 1$. If the pressure ratio is further increased to 2 or 3 (Fig. 4c, Fig. 4d) the cooling holes in the tip become choked. In the later case, the cooling effectiveness in the stagnation point rises to values above 0.3. When the distribution

of η_{ad} is compared with the trends predicted by the 1D model in Fig. 2b there agreement between both models can be seen. Fig. 5a shows a comparison between the laterally averaged adiabatic cooling effectiveness along the probe computed with both methods for pressure ratio values of $P_{0c}/P_{02} = [2,3]$. The region of rapid growth is well captured by the 1D model as well as the location and value of the point of maximum effectiveness. A noticeable difference occurs where the front window for optical access is placed, as the CFD values show a local drop in effectiveness that is not predicted by the 1D model, but still is within acceptable values. Additionally, for low pressures, the 1D model underpredicts the cooling effectiveness downstream the effusion faces, yielding more conservative results.

To characterize the effusion cooling performance of the probe for all its operating envelope, all the simulations introduced in Table 1 have been processed, η_{ad} has been averaged across the front effusion faces and plotted against the blowing ratio, defined in Eq 4. The coolant velocity is extracted from the total to static pressure ratio in the cooling holes as it dominates ejection in most of them. Fig. 5b shows a clear trend for $\overline{\eta_{ad}}$ with respect to blowing ratio at different Mach regimes, illustrating that the average effusion cooling effectiveness has much greater dependance on blowing ratio than on Mach number. There is a rapid rise in $\overline{\eta_{ad}}$ for low blowing ratios up to a threshold blowing ratio of 2 at which the effectiveness stabilizes around a value of 70% for all Mach regimes. However, despite a high overall effectiveness, the local effectiveness in the stagnation point of the tip will be almost null unless the pressure ratio for choking the holes in the tip is exceeded. This choking pressure ratio can be extracted from Fig. 5c and it is about ~1.5. In this study, it has been seen that choking the holes in the tip requires higher pressures than the ones required to reach the threshold blowing ratio of 2. Thus, the limiting condition for ensuring proper cooling in both the tip and the downstream surfaces becomes $P_{0c}/P_{02} > 1.5$. The one-dimensional model used to design the cooling jacket considered a cooling pressure of 3 bar, that yielded a pressure ratio of $P_{0c}/P_{02} = 2.3$, which satisfies this limiting condition, further supporting the proposed design.

$$BR = \frac{\rho_c U_c}{\rho_1 U_1} \tag{4}$$

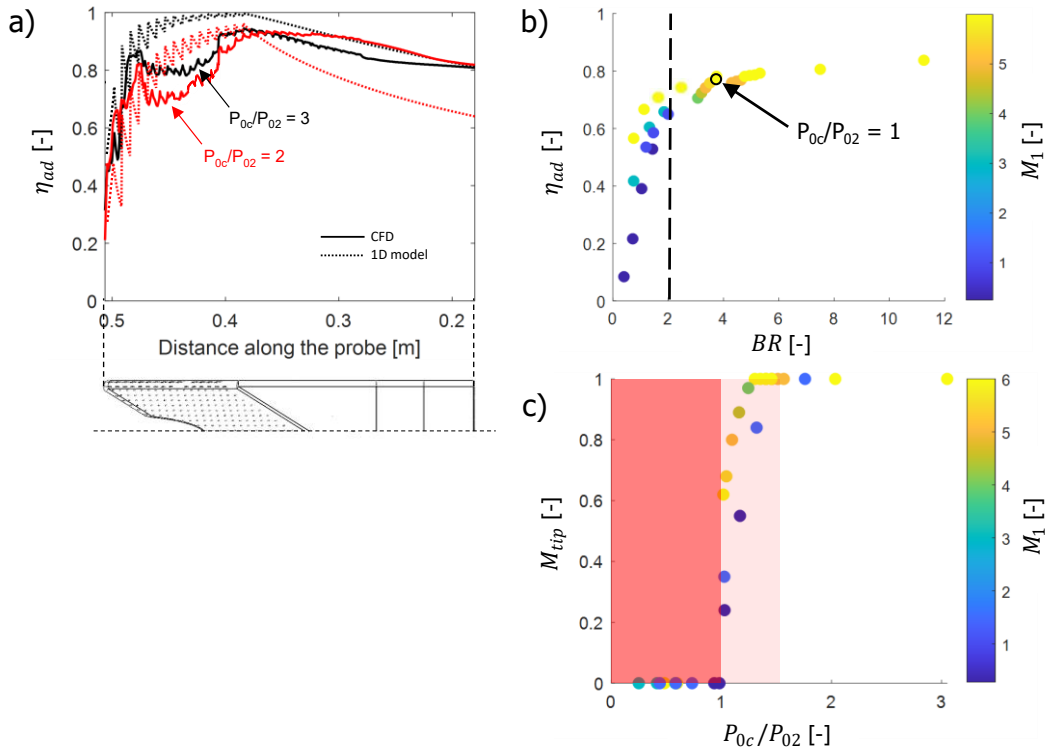

Fig 5. Comparison of η_{ad} between 1D model and CFD (a), and scatter plots of $\overline{\eta_{ad}}$ with respect to blowing ratio (b) and Mach number in the front holes depending on the pressure ratio (c) extracted from RANS simulations.

4. Experimental characterization of the cooling architecture

4.1. Experimental facilities

The cooling architecture of the probe was studied experimentally in the Open Jet facility of the Purdue Experimental Turbine Aerothermal Laboratory [21]. The Open Jet is a converging nozzle of 80 mm throat diameter that was operated at pressure ratios above the choking limit with total pressures between 2.05 and 2.2 bar to achieve underexpanded ejection and supersonic flow. Air from a 140 bar reservoir was passed through a natural gas heater to achieve a total temperature near 370 K to study the cooling effectiveness of the probe while not damaging sensitive instrumentation. The tip of the probe was positioned less than 10 cm away from the nozzle with the upper surface at 2 cm below the upper edge. Air was used as coolant and was injected through the plenum by a 40 mm diameter flexible hose with upstream total pressures up to 6 bar. However, pressure losses along the coolant-supply line and possible leakage reduced the maximum coolant pressure to 1.65 bar at the ejection holes. Three consecutive blowdowns were conducted, the first without cooling, and the remaining ones with coolant at total pressures of 1.29 and 1.65 bar measured at the effusion holes, yielding blowing ratios of 0.55 and 0.77 respectively. The experimental setup is shown in Fig. 6a. Fig. 6b shows the flow field produced by the underexpanded supersonic Open Jet from Schlieren diagnostics, and Fig. 6c shows a schematic of the instrumentation used, its placement, and the Field of View of the optical techniques.

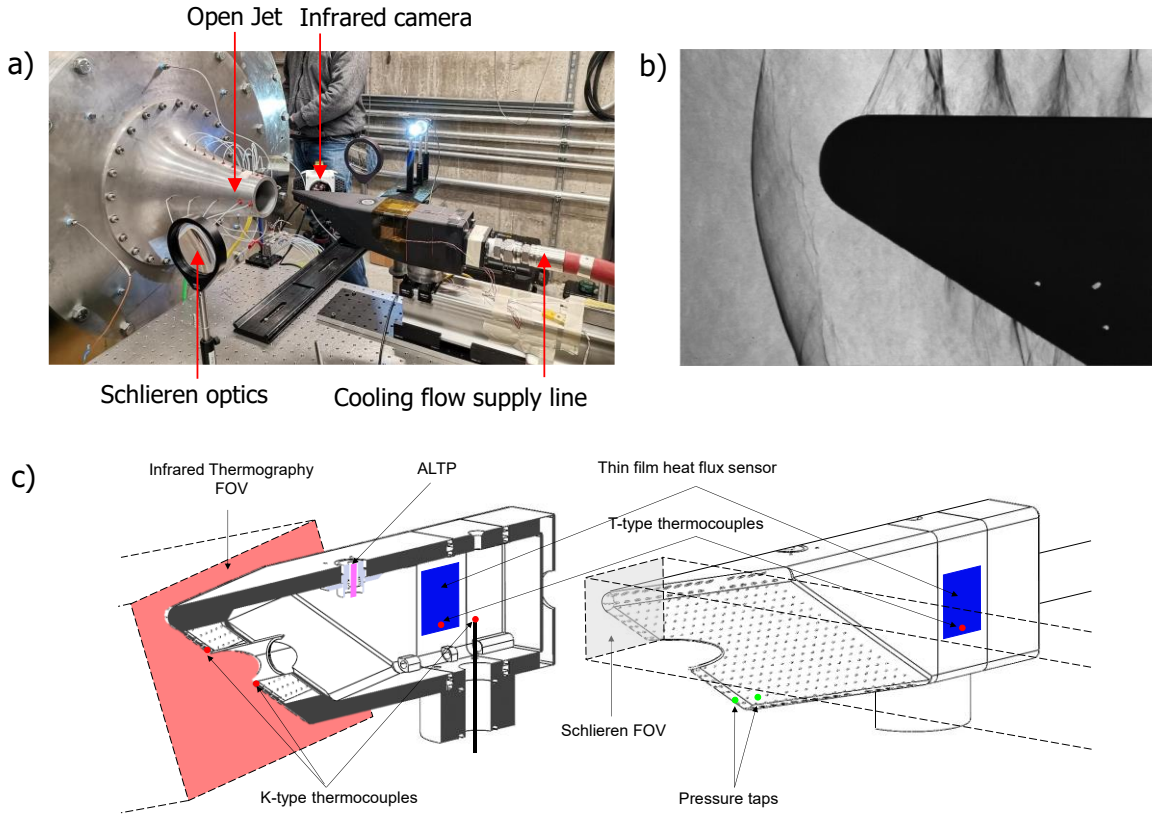

Fig 6. Probe installed downstream the Open Jet facility (a) with Schlieren image of the underexpanded test conditions (b) and schematic of the type and location of the instrumentation (c).

4.2. Data acquisition

K-type and T-type thermocouples were placed in the middle sections of the external, internal walls and inside the cavity, and two 100-μm thermocouple junctions were placed inside two front cooling holes, all connected to a VTI EX1048A conditioning system. Heat flux was measured across the internal and external surfaces with thin film heat flux sensors integrated with the T-type thermocouples. Pressure taps were introduced in two front effusion holes and connected to a ScaniValve MPS to monitor ejection pressure. The acquisition frequency of both systems was 800 Hz. Infrared Thermography (IR) was used to resolve spatial temperature profiles in the effusion faces with a Telops FAST-V1K camera. An acquisition frequency of 50 Hz and exposure time of 45 μs were chosen to reach 80% of maximum

pixel intensity at 370K, which was the maximum expected temperature in the test. The probe was coated in high-emissivity Cerakote.

4.3. Infrared thermography "in-situ" calibration

Despite the convenience of Infrared thermography for spatially resolving temperature-related magnitudes, a correlation between signal intensity at the camera chip and surface temperature must be made. Ostrowsky and Schiffer [22] noted that in fluid dynamics laboratory environments, physics-based models become inaccurate as not every affecting parameter can be accounted for, and proposed and "in-situ" non physics-based calibration approach. A pre-test is run covering the expected temperature range in different setpoints adding reference thermocouples at specific locations to calibrate the infrared readings. Based on the reference thermocouples, a surface fit is obtained at each calibration step, the infrared reading at each pixel is compared to the value of the surface fit, and a linear fit is applied to convert from uncorrected IR reading to surface temperature. The calibration coefficients are specific for each pixel, uncertainty can be quantified in the fit coefficients based on the goodness of fit and in the calibrated IR temperature using Taylor's uncertainty propagation [23]. This method needs to be applied at the exact same setup than the actual test to be able to use the same calibration coefficients. A detailed description of the method is shown by Ostrowsky and Schiffer [22].

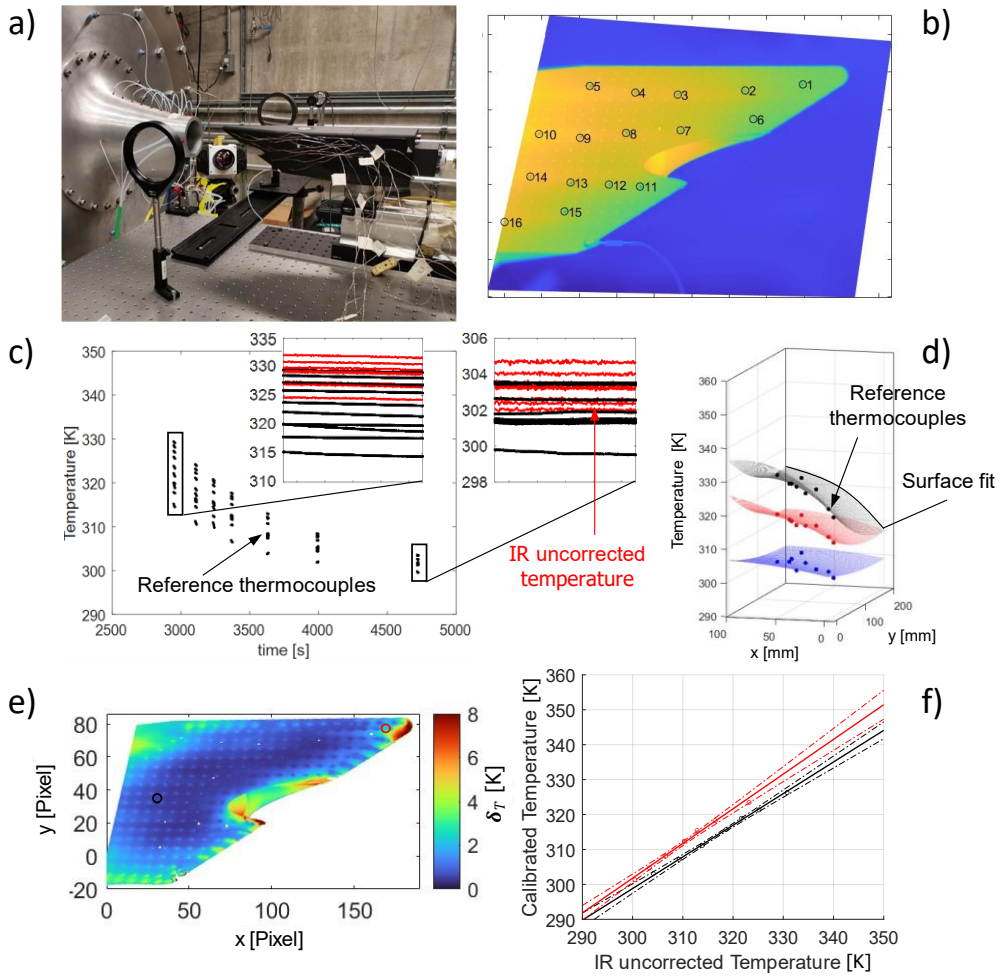

Fig. 7. Calibration setup (a) and spatial transformation of an IR image (b) with recorded temperature during calibration (c) and the surface fits (d), the uncertainty in the calibrated temperature for the fourth setpoint (e) and the straight line fit for two different pixels with uncertainty bounds (f).

The calibration was performed for the same setup than the test using a heat gun to supply heated flow through the plenum of the probe, heating symmetrically both sides of the probe allowing to instrument with thermocouples the effusion face that is "hidden" to the IR camera and use the readings as reference values for the opposite side. Fig. 7a shows the calibration setup with 10 K-type surface thermocouples. 16 silver dots were added at known locations to enable a spatial transformation

to correct for the camera view angle as shown in Fig. 7b. Using the heat gun, a maximum temperature of 340 K was reached in the effusion faces and 8 videos of 10 s were taken during the cooldown. Fig. 7c shows a comparison between the raw temperature readings (with the default calibration settings of the camera) and the reference thermocouples, where differences of 10 K were found at the highest temperature setpoint. Surface fits of second order in both directions were generated from the reference temperatures as shown in Fig. 7d and the uncertainty in the calibrated temperature for the highest temperature setpoint is shown in Fig. 7e, which is mostly kept below 1 K except by the high uncertainties in the tip. Finally, the straight-line calibration fit is found independently for each pixel, and it is shown in Fig. 7f for two different pixels circled in Fig. 7e with their corresponding uncertainty bounds. In the calibrated range, the uncertainty of a generic pixel is less than 2 K, but it can go beyond 5 K for temperatures beyond the calibrated ones. In the tests, only the tip will reach temperatures exceeding 345 K, so most of the probe lies within the bounds of the calibration.

4.4. Results

Temperature, pressure, and heat flux histories of the uncooled and the cooled blowdown at the highest blowing ratio ($BR = 0.77$) are shown in Fig. 8. Even for the low coolant pressures at the ejection holes (P_{0c} = 1.65 bar) the temperature inside the probe cavity increases less than 6 K with respect to no-flow conditions when the Open Jet flow reaches its highest temperature value of 360 K. Additionally, the heat flux measured through the internal wall is near 0 W/m^2 all along the test, validating the adiabatic assumption in the internal wall of the 1D model, and showing that the internal optics will not be exposed to high temperature gradients.

For each blowdown, the hot flow through the Open Jet necessitates time to reach stable temperatures as it dissipates heat to the walls of the settling chamber [24]. In order to extract steady information of the cooling effectiveness, the steadiness of the response at the end of the blowdowns is assessed. The derivative of wall temperature with time is evaluated at the tip of the probe from the IR recordings $\left(\frac{dT}{dt}\right)_{tip}$, and the slope at the final instant is shown in Table. 2. In the longest blowdown, quasi-steady state is reached as the slope is ~0.05 K/s (3 K/min) at the final instant. For cases 1 and 2, the slope is ~0.22 K/s and ~0.1 K/s respectively, which does imply a certain transient behavior in the response. However, if the third blowdown is used as reference, from the points at which its slope is 0.22 K/s and 0.1 K/s to the end of the blowdown, its temperature has only increased 5 K and 2.5 K respectively as the slope of the temperature response gets lower with time. The same behavior is expected for the first two runs, so the temperature at the end of each blowdown will be used for extracting quasi-steady information.

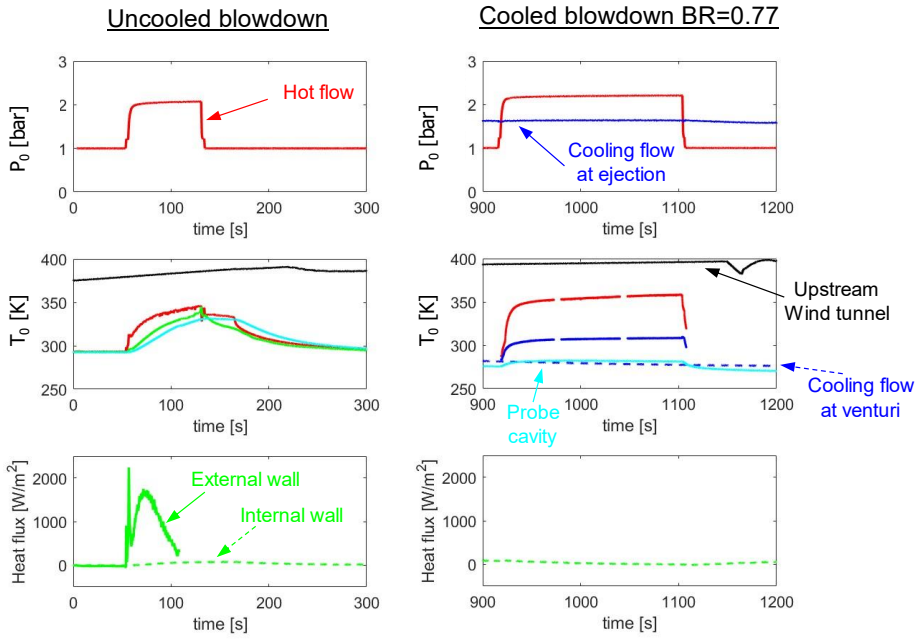

Fig 8. Pressure, temperature and heat flux history in the uncooled and cooled (BR=0.77) tests.

Table 2. Blowdown duration and temperature variation with time in the tip of the probe.

Blowdown	Duration (s)	$\left(\frac{dT}{dt}\right)_{tip}$ (K/s)
1. Uncooled	74.57	0.223
2. BR = 0.55	79.45	0.102
3. BR = 0.77	185.36	0.052

Fig. 9 shows the temperature profiles at the end of each blowdown. For all the conditions tested, the coolant pressure at ejection is lower than the total pressure of the hot flow (case 2: $P_{0c}/P_{02} = 0.6,$ and case 3: $P_{0c}/P_{02} = 0.75$), implying that no hole in the tip is ejecting. However, as shown in the numerical results of Fig. 4a, the rest of holes, oriented backwards, can eject, enhancing the cooling performance of the probe for low cooling pressures. Additionally, for the highest cooling pressure tested, the forward-ejecting holes below the tip can eject despite their low pressure. This behavior was also seen in the 3D RANS results of Fig. 4b for the same pressure ratio, further validating the numerical results.

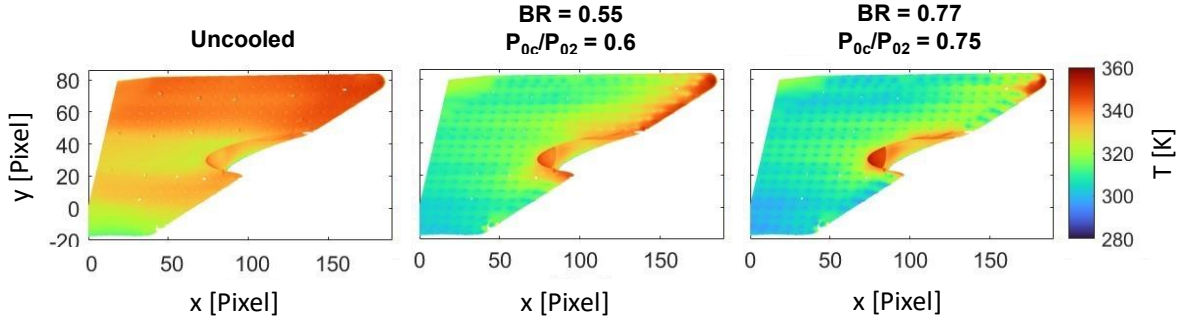

Fig 9. IR measured wall temperature for the uncooled, BR=0.55, and BR=0.77 cases.

To find the effusion cooling effectiveness, the same definition as in Eq 3 is used. However, the wall temperature measured in the cooled cases is not adiabatic as there is heat transfer through convection with the internal coolant. Thus, the value computed is the conjugate cooling effectiveness, shown in Eq 5, that overpredicts the adiabatic one due to the additional heat dissipation [25].

$$\eta_{cj} = \frac{(T_w)_{cooled} - (T_w)_{uncooled}}{T_{0c} - (T_w)_{uncooled}} \tag{5}$$

Fig. 10 shows η_{cj} contours for the two cooled cases. Near the left part of the images the ejected coolant has been able to form a film thick enough to prevent the hot flow from being in direct contact with the probe walls, reaching conjugate cooling effectiveness near 1. Additionally, a region of low η_{cj} appears immediately downstream of the front optical access port derived from the interaction between the access port and the hot flow. Both phenomena were also seen in the simulations in Fig. 4a, showing good agreement between simulations and experiments at nearly equal pressure ratios but highly different Mach numbers, as it was also seen in Fig. 5b**.**

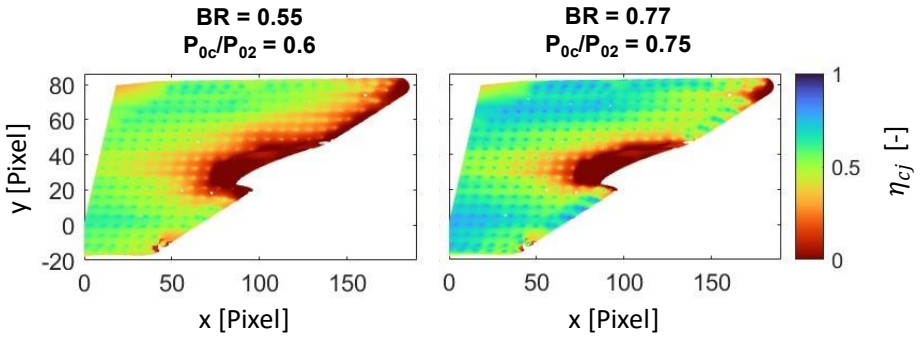

Fig 10. Conjugate cooling effectiveness for the blowdowns with BR=0.55 and BR=0.77.

The η_{cj} value averaged across the effusion wall is compared to the numerical results of $\overline{\eta_{ad}}$ in Fig. 11. A direct comparison is not possible due to the non-adiabatic effect of the conjugate effectiveness that is not captured in the adiabatic numerical simulations. However, the rapid rise in cooling effectiveness for low blowing ratios is accurately captured by the experimental results. For the measured blowing ratios, the experimental conjugate cooling effectiveness lies moderately above the trend for $\overline{\eta_{ad}}$ as the values are magnified due to the effect of internal convection cooling during the experiment. This further agreement with the numerical results validates the high-effectiveness trends predicted with the 1D and 3D RANS models and thus the ability of the designed architecture to cool the probe with moderately low cooling pressures.

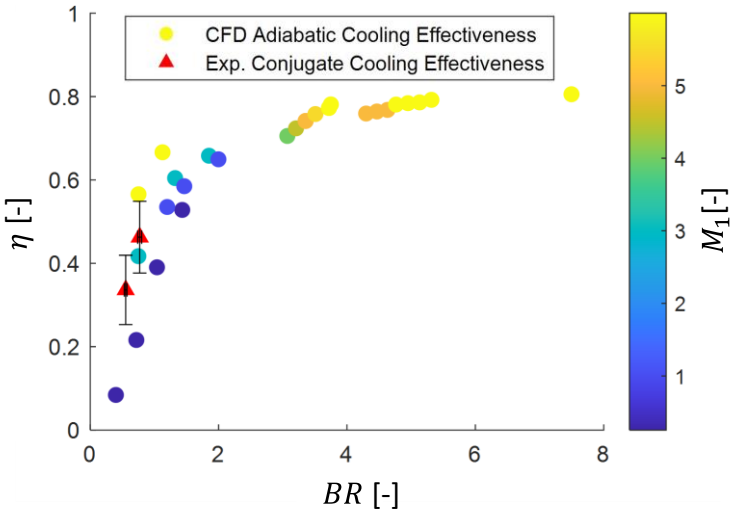

Fig 11. Average experimental conjugate cooling effectiveness compared with the average numerical adiabatic cooling effectiveness in terms of blowing ratio.

4.5. Uncertainty Propagation

The uncertainty in the calibrated IR temperature is computed from the uncertainty in the calibration coefficients of the linear fit as explained by Ostrowsky and Schiffer [22] assuming the thermocouples are the ground truth as they have been calibrated in a Fluke Calibration 9172 Field Metrology Wel between 273 and 373 K. The method proposed by Ostrowsky and Schiffer gives uncertainty values for each pixel that vary with the temperature read. The uncertainty in η_{cj} can be found using Taylor's uncertainty propagation for each pixel in the two frames of Fig. 10 with Eq 6 [23]. The uncertainty of the spatially averaged effectiveness is the average of the pixel uncertainties as shown in Eq 7. Taylor's propagation formulas have also been used to compute the uncertainty in the blowing ratio for each blowdown. These values are shown in Table 3 and give the error bars used in Fig. 11.

$$\delta^2{}_{\eta_{cj}} \approx \frac{\delta^2{}_{(T_w)_{cooled}} + \delta^2{}_{(T_w)_{uncooled}}}{[T_{0c} - (T_w)_{uncooled}]^2} + \frac{[(T_w)_{cooled} - (T_w)_{uncooled}]^2}{[T_{0c} - (T_w)_{uncooled}]^4} \cdot \left(\delta^2{}_{T_{0c}} + \delta^2{}_{(T_w)_{uncooled}}\right) \quad (6)$$

$$\delta_{\overline{\eta_{cj}}} = \frac{1}{N}\sum_{i=1}^{N} \delta_{(\eta_{cj})_i} \quad (7)$$

Table 3. Mean values and uncertainties

BR [−]	δ_{BR} [−]	$\overline{\eta_{cj}}$ [−]	$\delta_{\overline{\eta_{cj}}}$ [−]
0.55	0.022	0.33	0.083
0.77	0.031	0.46	0.086

5. Conclusion

A cooled probe has been designed to house sensitive instrumentation for optical diagnostics in high-enthalpy facilities operating under conditions up to a most severe scenario of $M_1 = 6$, $T_{01} = 1700\ K$, $P_{01} = 45$ bar. An open-cycle gaseous system is used that effectively refrigerates a 980 cm^3 cavity with the necessary volume and access ports to enclose components for performing optical diagnostics in facilities with low optical access. A 1D heat transfer model is used for sizing the cooling jacket accounting for convection, conduction, and effusion cooling phenomena resulting in a structure that can be cooled with a head pressure of 3 bar in the most severe scenario satisfying the material limits (800 K) and the temperature restrictions inside the cavity (315 K). A significant reduction in wall temperature was seen due to effusion cooling which was confirmed through 3D steady RANS simulations. For total pressure ratios exceeding unity, effusion cooling reached a cooling effectiveness close to 100% at the middle of the probe. However, pressure ratios higher than 1.5 are required to choke the front holes and start seeing an effect in the tip region. This condition was satisfied by the 1D model, supporting the proposed design. A global trend is shown for the average adiabatic cooling effectiveness depending on blowing ratio that reveals low dependence on the Mach number.

Experimental tests conducted in an Open Jet blowdown facility at underexpanded $M_1 = 1.07$ conditions near 370 K corroborate the numerical findings. Infrared thermography, combined with an "in-situ" calibration procedure enabled the resolution of temperature fields in the effusion faces and the calculation of conjugate cooling effectiveness. Features observed in the test such as the activation of forward-ejecting holes were seen in the simulations at Mach 6 at similar pressure ratios, confirming the ability to use the data collected in the test to understand the operation of the probe at higher Mach numbers. Additionally, the experimental values of the average cooling effectiveness follow the same behavior with blowing ratio than the numerical results. The agreement shown between 1D model, steady RANS simulations and experimental tests support the ability of the cooling design to satisfy the temperature requirements of the probe even at $M_1 = 6$, $T_{01} = 1700\ K$, $P_{01} = 45$ bar.

References

1. Viguier, P., Garraud, J., Soutade, J., Serre, L., Defoort, S., Ferrier, M., Ristori, A.: Development of f4 hotshot windtunnel for high enthalpy scramjet tests. In: 18th AIAA/3AF International Space Planes and Hypersonic Systems and Technologies Conference. p. 5970 (2012)
2. Serre, L., Denis, P., Cortes, N., Falempin, F.: Development of S4 free jet test facility for the French Lea flight test program. In: 17th AIAA International Space Planes and Hypersonic Systems and Technologies Conference. p. 2264 (2011)
3. Inman, J.A., Bathel, B.F., Johansen, C.T., Danehy, P.M., Jones, S.B., Gragg, J.G., Splinter, S.C.: Nitric-oxide planar laser-induced fluorescence measurements in the hypersonic materials environmental test system. AIAA journal. 51, 2365–2379 (2013)
4. Brouckaert, J.-F., Mersinligil, M., Pau, M.: A conceptual design study for a new high temperature fast response cooled total pressure probe. (2009)
5. Bogard, D.G., Thole, K.A.: Gas turbine film cooling. J Propuls Power. 22, 249–270 (2006)
6. Bahr, D.W.: Aircraft Turbine Engine Combustors-Development Status/Challenges. In: Combustings Flow Diagnostics. pp. 357–374. Springer (1992)
7. Gustafsson, K.M.B.: Experimental studies of effusion cooling. Citeseer (2001)
8. Chuvakhov, P. V: Investigation of heat flux and effusion/film cooling efficiency over a sharp cone surface at high supersonic speeds. In: 29th Congress of the International Council of the Aeronautical Sciences, ICAS 2014 (2014)
9. Lozano, F., Paniagua, G.: Airfoil leading edge blowing to control bow shock waves. Sci Rep. 10, 21922 (2020)
10. McKelvy, A.: High Precision Force Application and Temperature Resistant Probe Nacelles for Supersonic Exhaust Characterization, (2021)
11. Incropera, F.P., DeWitt, D.P., Bergman, T.L., Lavine, A.S.: Fundamentals of heat and mass transfer. Wiley New York (1996)
12. Winterton, R.H.S.: Where did the Dittus and Boelter equation come from? Int J Heat Mass Transf. 41, 809–810 (1998)

13. Colban, W.F., Thole, K.A., Bogard, D.: A film-cooling correlation for shaped holes on a flat-plate surface. (2011)
14. Sellers Jr, J.P.: Gaseous film cooling with multiple injection stations. AIAA Journal. 1, 2154–2156 (1963)
15. Goldstein, R.J.: Film cooling. In: Advances in heat transfer. pp. 321–379. Elsevier (1971)
16. Chakravarthy, S., Peroomian, O., Goldberg, U., Palaniswamy, S.: The CFD++ computational fluid dynamics software suite. In: AIAA and SAE, 1998 World Aviation Conference. p. 5564 (1998)
17. South, J.C.: Calculation of Axisymmetric Supersonic Flow Past Blunt Bodies with Sonic Corners: Including a Program Description and Listing. National Aeronautics and Space Administration (1968)
18. Krasil'nikov, A. V, Nikulin, A.N., Kholodov, A.S.: Some features of flow over spherically blunted cones of large vertex angles. Izv. Akad. Nauk SSSR Mekh. Zhidk. Gaza. 2, 179–181 (1975)
19. Zhang, W., Zhang, Z., Wang, X., Su, T.: A review of the mathematical modeling of equilibrium and nonequilibrium hypersonic flows. Advances in Aerodynamics. 4, 38 (2022)
20. Kantrowitz, A.: Preliminary investigation of supersonic diffusers. National Advisory Committee for Aeronautics (1945)
21. Paniagua, G., Cuadrado, D., Saavedra, J., Andreoli, V., Meyer, T., Solano, J.P., Herrero, R., Meyer, S., Lawrence, D.: Design of the Purdue experimental turbine aerothermal laboratory for optical and surface aerothermal measurements. J Eng Gas Turbine Power. 141, 012601 (2019)
22. Ostrowski, T., Schiffer, H.P.: High-resolution heat transfer measurements on a rotating turbine endwall with infrared thermography. Meas Sci Technol. 32, 125207 (2021)
23. Taylor, J.R., Thompson, W.: An introduction to error analysis: the study of uncertainties in physical measurements. Springer (1982)
24. Saavedra, J., Paniagua, G., Lozano, F., Fisher, J., Webb, A., Meyer, T.: Flow conditioning system for tri-sonic high pressure aerothermal testing. Flow Measurement and Instrumentation. 79, 101910 (2021)
25. Lu, X., Jiang, P., Sugishita, H., Uechi, H., Suenaga, K.: Conjugate heat transfer analysis of film cooling flows. Journal of Thermal Science. 15, 85–91 (2006)